Computers and Concrete, *Vol. 24, No. 1 (2019) 37-49*
DOI: https://doi.org/10.12989/cac.2019.24.1.037

Shear behaviour of RC beams retrofitted using UHPFRC panels epoxied to the sides

Mohammed A. Al-Osta*

Department of Civil & Environmental Engineering, King Fahd University of Petroleum & Minerals (KFUPM), Dhahran 31261, Saudi Arabia

(Received May 29, 2018, Revised March 24, 2019, Accepted May 11, 2019)

Abstract. In this study, the shear behaviour of reinforced concrete (RC) beams that were retrofitted using precast panels of ultra-high performance fiber reinforced concrete (UHPFRC) is presented. The precast UHPFRC panels were glued to the side surfaces of RC beams using epoxy adhesive in two different configurations: (i) retrofitting two sides, and (ii) retrofitting three sides. Experimental tests on the adhesive bond were conducted to estimate the bond capacity between the UHPFRC and normal concrete. All the specimens were tested in shear under varying levels of shear span-to-depth ratio (*a/d*=1.0; 1.5). For both types of configuration, the retrofitted specimens exhibited a significant improvement in terms of stiffness, load carrying capacity and failure mode. In addition, the UHPFRC retrofitting panels glued in three-sides shifted the failure from brittle shear to a more ductile flexural failure with enhancing the shear capacity up to 70%. This was more noticeable in beams that were tested with *a/d*=1.5. An approach for the approximation of the failure capacity of the retrofitted RC beams was evolved using a multi-level regression of the data obtained from the experimental work. The predicted values of strength have been validated by comparing them with the available test data. In addition, a 3-D finite element model (FEM) was developed to estimate the failure load and overall behaviour of the retrofitted beams. The FEM of the retrofitted beams was conducted using the non-linear finite element software ABAQUS.

Keywords: ultra-high performance fiber reinforced concrete; shear behaviour; retrofitting; epoxy agglutinant; bond capacity; failure mode; finite element model

1. Introduction

Reinforced concrete (RC) is a vital material in the construction of structures around the world. RC structures exhibit admirable performance in respect of their mechanical properties, durability and economy. However, over time, RC structural elements are usually affected by numerous problems, such as the corrosion of steel rebars, increased loads, exposure to aggressive environments and changes in the usage of the structures. Therefore, one of the many challenges in civil infrastructure engineering is to repair or strengthen these structural elements whenever necessary. Many research studies have been conducted into the rehabilitation of RC structures, while new materials have been emerged to restore and improve the damaged members. The most popular technique is the use of carbon fiber reinforced polymer (CFRP) laminates for upgrading the deteriorated structures. CFRP possesses valuable properties, such as high capacity, corrosion protection, simplicity of application and minimal size change. In spite of these advantages, a CFRP repair system does have certain shortcomings, mainly related to bond and incompatibility issues (Mohammed *et al.* 2016). Consequently, various types of concrete have been developed through extensive research endeavors. Most of these new types of concrete were developed to overcome the shortcomings of CFRP. One of these newly developed types of concrete is ultra-high performance fibre reinforced concrete (UHPFRC). Most researchers recognize excellent suitability and capability of using UHPFRC for the rehabilitation and retrofitting of existing RC structures. The advantages of using UHPFRC include the enhancement of durability and the overall serviceability of structures, high bond strength and ease of application.

Many research works have been accomplished on both the mechanical properties and durability of UHPFRC, demonstrating the excellent performance of UHPFRC (Rahman *et al.* 2005, Graybeal 2011, Graybeal 2006, Ahlborn *et al.* 2011, Tai *et al.* 2011). It was reported that UHPFRC could have a compressive strength exceeding 170 MPa; a tensile strength of over 8 MPa; and a flexural strength of more than 30 MPa (Lubbers 2003, Hakeem 2011, Al-Osta 2018). The composition of UHPFRC includes sand, cement, silica fume, water, super-plasticizer and chopped high-strength steel fibers, which is necessary to obtain ductile behaviour of the fiber-matrix composite. The matrix is responsible for the homogeneity and low permeability of the UHPFRC. UHPFRC is versatile and can be applied on either existing or newly-built structures. It can be cast on normal concrete members in different configurations, either on tensile or compressive faces.

In the area of repair and retrofitting of structural elements, enormous number of research studies have been

*Corresponding author, Assistant Professor
E-mail: malosta@kfupm.edu.sa

ISSN: 1598-8198 (Print), 1598-818X (Online)

carried out on the repair and retrofitting of RC concrete elements using several types of high performance concretes. Noshiravani and Brühwiler (2013) studied the response of composite beams made with 50 mm thick reinforced UHPFRC (R-UHPFRC) and 250 mm deep RC and subjected them to combined loading (bending and shear). This study concluded that the addition of a R-UHPFRC layer at the tension face is an effective shear strengthening technique. Ruano *et al.* (2014) conducted an experimental investigation of the shear performance of RC beams that were retrofitted using steel fiber reinforced concrete (SFRC) with different dosages of fiber (30 kg/m^3 and 60 kg/m^3). The experimental results confirmed that the use of fiber generally enhanced the integrity of the retrofitted RC beams. Ombres (2015) investigated the behaviour of RC beams retrofitted in shear with a fabric reinforced cementitious matrix (FRCM). The fibers of the FRCM system were made of PBO (Polypara-phenylene-benzo bisthiazole) meshes. Two configurations of FRCM strips (U-wrapped continuous and discontinuous) were considered. The results showed that the FRCM strengthening method increased the shear capacity of the RC beam when an adequate strengthening configuration is adopted. Ruano *et al.* (2015) studied experimentally and numerically the impact of high-performance self-compacting concrete (HP-SCC) as a strengthening material for RC beams in shear. The results indicated that higher fiber content increased the failure load and enhanced the bond between the normal concrete and HP-SCC in the retrofitted RC elements. Chalioris *et al.* (2014) reported the effect of using a layer of reinforced self-compacting concrete (SCC) on the shear performance of retrofitted RC beams. The results demonstrated that the use of SCC as a strengthening material would increase the capacity, as well as improve the ductility, of a retrofitted RC beam. Hussein and Amleh (2015) studied the behavior of members made with UHPFRC, normal strength concrete (NSC), and high strength concrete (HSC). Both the flexural and shear behaviours were investigated. The composite beams exhibited significantly high flexural and shear capacities, as well as high ductility. Mohammed *et al.* (2016) studied the effect of using UHPFRC as a strengthening material for RC beams without stirrups under torsional loading. The results showed that the use of UHPFRC on all longitudinal sides of the RC beams would enhance the torsional strength of the RC beams. Several other studies have been reported to use finite element modelling to study the performance and predict the failure loads as well as the modes of failure of retrofitted RC Beams (Chen and Tao 2011, Khan *et al.* 2017, Al-Osta *et al.* 2017, Bahraq *et al.* 2019). It was observed that the concrete damage plasticity model is the most commonly model used for simulation of concrete.

Literature review has shown that limited studies have been reported on the shear behaviour of RC beams retrofitted with precast panels of cement-based composite materials. Hence, this study reports experimental and analytical studies conducted to investigate the effect of varying the shear span-to-depth ratio (*a/d*) and retrofitting configurations on the shear response of RC beams retrofitted with precast UHPFRC panels that were attached to the RC beams using epoxy adhesive.

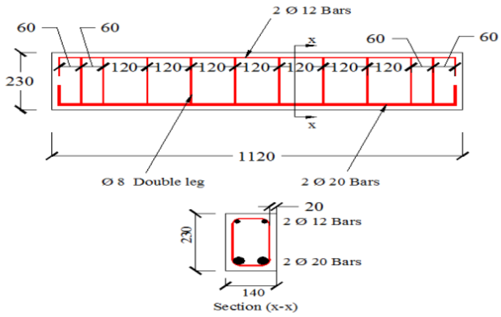

Fig. 1 Details of concrete beam specimens (all dimensions in mm)

2. Experimental work

The experimental work included material strength tests for normal concrete (NC), UHPFRC, and steel rebar, in addition to a shear strength test for RC beam specimens before and after retrofitting with UHPFRC panels, and experimental tests on the adhesive bond between NC and UHPFRC. The material strength tests involved the uniaxial stress-strain test in tension and compression for both UHPFRC and NC. For the steel rebar, a uniaxial stress-strain test in tension was carried out. The data obtained from the material strength tests were used in developing a 3-D finite element model (FEM) of the beams, as well as to furnish a clear understanding of the shear performance of the RC beams. The bond strength between UHPFRC and NC was evaluated by conducting slant shear and split tensile strength tests on the composite cylinders. Finally, both unretrofitted and retrofitted beam specimens were tested with varying *a/d*.

2.1 Specimen preparation

Six RC beams measuring 140 × 230 × 1120 mm were designed and fabricated. The tested beam specimens were designed (according to ACI 318-14) in such a way to make sure their failure is in shear. The details of the steel reinforcement in the beam specimens are shown in Fig. 1. A clear cover of concrete of 20 mm to the steel bars was used. The main longitudinal steel rebars consist of two bars in bottom and top with 20 mm and 12 mm diameter bars, respectively. The stirrups were 2-legged 8 mm diameter steel bars at a spacing of 120 mm center to center, as shown in Fig. 1. All tested specimens and experimental variables are shown in Table 1. Two of the beam specimens were tested as control specimens, whereas the remaining four specimens were tested after retrofitting with various configurations using UHPFRC retrofitting panels with a thickness of 30 mm. The specimens marked with 'CT' stand for control, while 'SJ' represents the RC beam after retrofitting. The designations used in Table 1 also reflect *a/d* ratios and the retrofitting configurations (two and three sides). For example, specimen RC 2SJ 1.0 was tested with *a/d*=1.0 and was retrofitted with two longitudinal vertical UHPFRC layers. To ensure quality control of the NC used, the beams were prepared and cast in a commercial precast concrete plant.

Table 1 Details of the tested beam specimens

Specimen Designation	Dimensions* $b\times h\times L$ [mm]	*a/d* Ratio	Shear Span [mm]	Beam Description
RC-CT-1.0	140×230×1120	1.0	200	Control beam
RC-2SJ-1.0	200×230×1120			Beam retrofitted by two UHPFRC vertical panels **epoxied** to the sides
RC-3SJ-1.0	200×260×1120			Beam retrofitted by UHPFRC panels **epoxied** to the sides, two vertical and one bottom
RC-CT-1.5	140×230×1120	1.5	280	Control beam
RC-2SJ-1.5	200×230×1120			Beam retrofitted by two UHPFRC vertical panels **epoxied** to the sides
RC-3SJ-1.5	200×260×1120			Beam retrofitted by UHPFRC panels **epoxied** to the sides, two vertical and one bottom

*The dimensions b and h for RC-2SJ and RC-3SJ include the thickness of UHPFRC panels (30 mm).

Table 2 Specimen descriptions for the properties of materials

Material	Test Type	Specimen Size
NC	Compressive strength	75×150 mm cylinder
	Modulus of elasticity	75×150 mm cylinder
UHPFRC	Compressive strength	50×50×50 mm cube
	Stress-strain behaviour and modulus of elasticity	75×150 mm cylinder
	Direct tension	390×120×40 mm dogbone
	Flexural strength	40×40×160 mm prism
Composite NC/UHPFRC	Splitting tensile strength	75×150 mm composite cylinder
	Slant shear strength	75×150 mm composite cylinder
Steel Reinforcement	Direct tension	Ø 8, Ø 12, Ø 20

Table 3 UHPFRC mix design (Ahmad *et al.* 2016)

Material	Mix Proportion (kg/m^3)
Cement	900
Dune sand	1005
Micro-silica	220
Superplasticizer	40.3
Steel fibers	157
Water	162.4

Fig. 2 Test setup for flexural strength test of UHPFRC

2.2 Material properties

Small-scale specimens were prepared and different standardized tests were conducted to characterize material properties. Table 2 illustrates the specimens' details and test methodologies that were used to obtain the mechanical properties of the materials used in the fabrication, repairing and retrofitting of RC beam specimens. The test of bond was also preformed to estimate the bond capacity between the NC substrate and UHPFRC.

2.2.1 Steel reinforcing bars

The mechanical properties of steel rebars used in RC beams were obtained by testing three samples from each diameter under uniaxial tension. The average yield stress obtained for steel rebars of 20 mm, 12 mm and 8 mm diameter bars are f_y=610, 610 and 600 MPa, and the average ultimate strength of f_u=710, 710 and 690 MPa, respectively. The elastic modulus of all bars is E_s=200,000 MPa.

2.2.2 Normal Concrete (NC)

The compressive strength tests of NC were conducted according to ASTM C39 (ASTM International 2017) on a 75×150 mm cylinder. The splitting tensile tests were conducted for NC according to ASTM C496 (ASTM International 2004). The average values of compressive and splitting strengths after 28 days for the cylinder of NC were f_c'=65 MPa and ft_{sp}=4.81 MPa, respectively.

2.2.3 UHPFRC

The UHPFRC, which is a class of ultra-high strength concrete, was recently developed based on the utilization of ultra-fine materials, such as micro-silica, and incorporation of relatively high volume of steel fibres. The mix design of UHPFRC used in this study is similar to that in Ref. (Ahmad *et al.* 2016) and shown in Table 3. Two different sizes of steel fibers were used i.e., 50% of straight fibers and 50% of hooked fibers. This is a common formulation of fiber mixture utilized in UHPFRC. It is called 'fiber cocktail'. The dimensions of hooked steel fibers are a 0.2 mm diameter and 25 mm length, while the straight steel fibers had a diameter of 0.1 and a length of 12.5 mm. The tensile strength of both hooked-end and straight steel fibers is 2500 MPa. The flexural strength of UHPFRC was performed according to ASTM C78 (ASTM International 2017), with four points of flexural loading on the prism having a size 40×40×160 mm, as shown in Fig. 2. The compressive behaviour of UHPFRC was obtained by testing

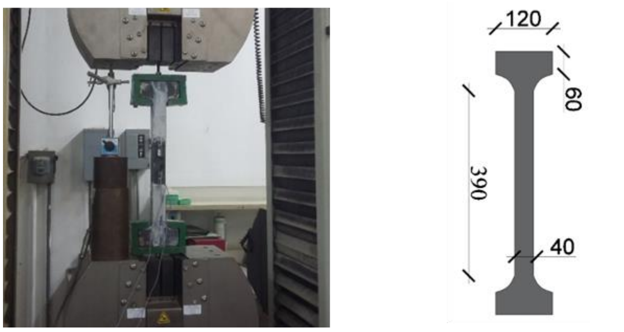

Fig. 3 Test setup for direct tensile strength test (all dimensions in mm)

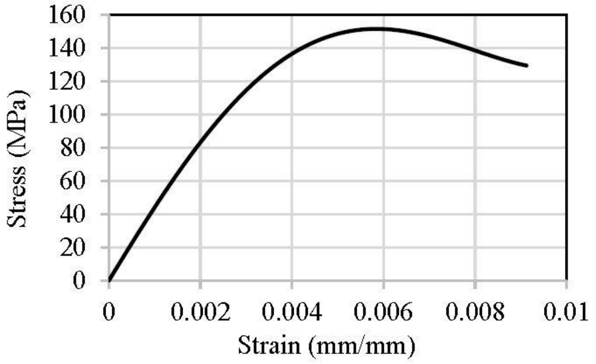

(a)

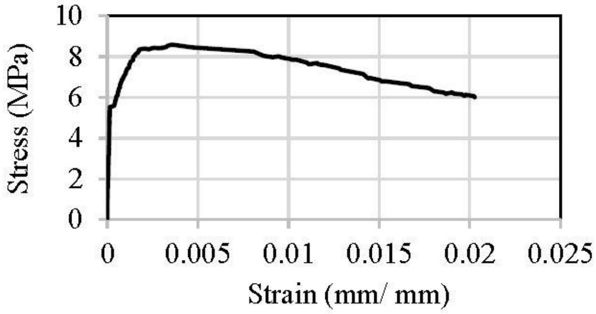

(b)

Fig. 4 Behaviour of UHPFRC in (a) compression and (b) tension

the cylindrical specimens in the compression machine (ASTM- C469), which has an ultimate capacity of 3000 kN, and the load was applied at a rate of 1.5 kN/sec. With regards to the tensile response of UHPFRC, the dogbone specimens with square cross-section was prepared, as shown in Fig. 3. These specimens were tested under the direct tensile load at a rate of 0.5 mm/min and the loads were recorded in displacement-control setup (0.05 mm).

The full setup of the uniaxial tensile test on a dogbone specimen is also shown in Fig. 3. Fig. 4 displays the stress-strain behaviour of the material under uniaxial compression and tension test. The cylindrical specimens of UHPFRC were tested at 28-days and the average compressive strength and modulus of elasticity were found to be f_{uc}=151.4 MPa and E_{UHPFRC}=41 GPa, respectively. The average flexural and tensile strengths at 28 days for the prism and dogbone specimens of UHPFRC were 25.4 MPa and 8.6 MPa, respectively.

Table 4 Mechanical properties of epoxy primer (Sika Construction Chemicals 2014)

Properties	Curing Time (days)	Curing Temperature		
		+23℃	+30℃	+40℃
Compressive Strength (MPa)	14	~39	~43	~56
Flexural strength (MPa)		~38	~38	~42
Tensile Strength (MPa)		~22	~24	~25
Bond Strength (MPa)	7	>3	-	-
Tensile E-modulus (MPa)	14	~2750	-	-
Flexural E-modulus (MPa)		~2600		
Compressive E-modulus (MPa)		~2100		

2.2.4 Epoxy

For enhancing the structural capacity of the RC beams, pre-fabricated UHPFRC panels were attached to NC using Sikadur® -32 LP (Sika Construction Chemicals 2014). This is a two-part (part A and part B) structural epoxy bonding agent and adhesive for concrete elements and it has to be mixed and used at temperatures between 23℃ and 40℃. The curing time of Sikadur® -32 LP ranges between 7 to 14 days at a room temperature of 23℃. The mechanical properties of the epoxy bonding over seven days of curing (23℃) were reported by the manufacturer as (Sika Construction Chemicals 2014): compressive strength of 38 MPa; flexural strength of 38 MPa; tensile strength of 22 MPa; and bond strength of 3 MPa. The mechanical properties, as obtained from the product data sheet, are presented in Table 4.

2.2.5 Bond strength of composite NC/UHPFRC

The bond quality of composite materials (NC and UHPFRC) in a retrofitting technique (epoxy-adhesive) was assessed by conducting bond tests according to ACI-546 (ACI 546.3R-14 2014). These tests were the splitting tensile and slant shear strength tests. A total of twelve composite cylinders were made of NC and UHPFRC in two different arrangements, either in a vertical plane (at 90°) or in a slant plane (at 30°). Before applying the epoxy adhesive (Sikadur® -32 LP Epoxy Bonding Agent), the exposed surfaces were cleaned and prepared using grinding.

The composite cylindrical specimens in the splitting tensile test were tested according to ASTM C496 (ASTM International 2004), as can be seen in Fig. 5(a). The failure modes of the samples after testing are shown in Fig. 5(a). The splitting tensile capacity, σ_t, of the composite sample load can be estimated by $\sigma_t=2P/\pi A$. Where: σ_t=splitting tensile capacity, MPa; P=maximum applied load, N; A= area of the bonding plane, mm^2.

The composite specimens in the slant shear test were tested according to ASTM C882 (ASTM International 2013) as can be seen in Fig. 5(b). The modes of failure of specimens under the slant shear test is shown in Fig. 5(b). The compressive strength of the composite specimen was determined using the collapse load and elliptical area of bond between the NC and UHPFRC.

The failure of the tested composite cylinders showed a substrate-failure for those specimens, which were bonded

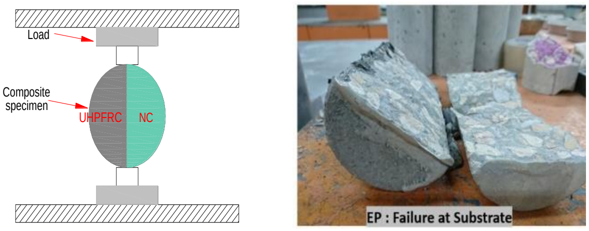

(a)

(b)

Fig. 5 (a) Splitting tensile test, (b) Slant shear test

Table 5 Retrofitting schemes of beams specimens

Retrofitting Configurations (Thickness of UHPFRC Jacket=30 mm)	
Retrofitting Pattern	Specimen Identification
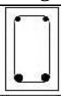	RC- CT
	Two sides jacketing(2*SJ*) (RC-2SJ)
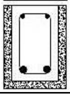	Three sides jacketing(3*SJ*) (RC-3SJ)

using an epoxy adhesive. On top of that, the substrate failure was explosive and the epoxy bonding was not affected by either the high compression or shear stresses (in the slant shear test) or tensile stresses (in the splitting tensile test), as shown in Figs. 5(a) and 5(b). The composite specimens exhibited an excellent bonding behaviour under both tests.

The average values of the splitting tensile and slant shear strengths of the tested cylindrical specimens were 8.3 MPa and 26.5 MPa, respectively. Therefore, the splitting tensile strength of the cylindrical specimens were found to be within the category of “Excellent bond value” (i.e., for tensile bond strength≥2.1 MPa) as measured by Sprinkel and Ozyildirim (2000). In addition, the results of the slant shear test indicated an adequate bond strength when compared to the results reported by Chynoweth *et al.* (1996) which specified a minimum slant shear strength of 20.7 MPa. Accordingly, the epoxy bonding between the substrate and overlay of UHPFRC can be classified in the category of an excellent bonding strength.

2.3 Retrofitting configurations

The RC beams were retrofitted for shear by casting panels of UHPFRC with a thickness of 30 mm and bonding them using an epoxy adhesive to the surface of the RC

Fig. 6 Procedure for epoxy technique

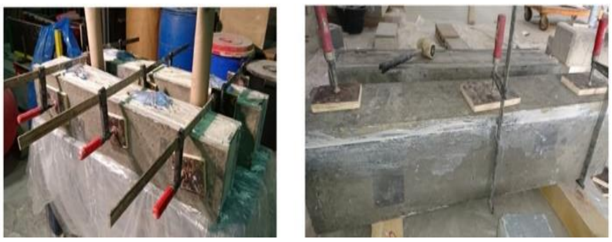

(a) (b)

Fig. 7 Applying the retrofitted strips to the beam substrate: (a) RC-2SJ, (b) RC-3SJ

beams in the configurations shown in Table 5. In this technique of retrofitting, UHPFRC strips were cast separately and cured for 28 days. The substrate and the surface of the UHPFRC strips were cleaned and prepared using grinding and with sandpaper, as shown in Fig. 6. Thereafter, a special adhesive epoxy (commercially known as Sikadur-32LP 2-Part Structural Epoxy Bonding Agent) was used and the two parts of the epoxy were mixed according to the manufacturer’s recommendation. The epoxy was applied on the surfaces with an approximate thickness of 1.5 mm (2.1 kg/m^2) and the retrofitted strips were bonded to the beams. Steel clamps were used to fix the retrofitted strips onto the substrate and to ensure a uniform level of adhesion, Fig. 7. Different configurations were used (either two-side jacketing or U-jacketing). Consequently, the retrofitted beams were cured for 7 days at a temperature of 23°C in order to develop the full bond-strength according to the manufacturer’s recommendation (Sika Construction Chemicals 2014).

2.4 Beam shear strength tests

A total of six RC beam specimens were cast, cured and tested using a four-point loading preparation, as shown in Fig. 8. To measure the midspan deflection, a linear variable differential transformer (LVDT) was attached to the bottom face of the tested beam. Two LVDT’s located at the

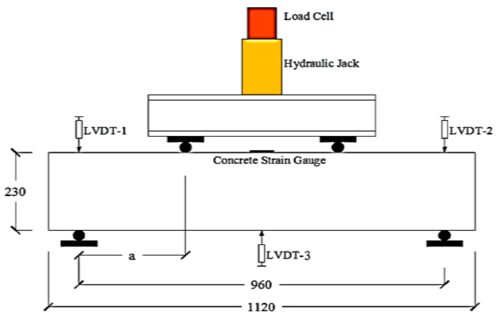

Fig. 8 Schematic representation of beam testing setup (all dimensions in mm)

supports on the top face of the tested beams were used to measure the rotations at the supports. A strain gauge for the concrete was used in the midspan of the top beam to measure the strain of the concrete. Similarly, strain gauges for the steel were glued to reinforcing bars and used to measure the deformation in the reinforcing steel. The beams were tested under a displacement-control load at a rate of 0.5 mm/min until collapse. All of the needed data were recoded such as the load vs. deflection curves, the first cracks and the failure modes.

3. Finite element model

A 3D finite element model (FEM) was developed to simulate the shear behaviour of the retrofitted RC beam including modelling the NC, UHPFRC and the reinforcing steel rebars, as well as the bond between the NC and the UHPFRC surfaces. The effect of varying *a/d* ratios and

Table 6 CDP model parameter for NC and UHPFRC

Dilatation angle Ψ (°)	Flow potential eccentricity ε	σ_{b0}/σ_{c0}	K	viscosity parameter
36	0.1	1.16	0.67	0

strength configurations on the shear behaviour of the retrofitted RC was also demonstrated. The displacement control loading was used to apply the load up to failure. In this study, the ABAQUS software was utilized to simulate the behaviour of RC beams, while dynamic explicit analysis was used to avoid the convergence problem accompanying the cracking of the concrete and the de-bonding of the UHPFRC. This type of analysis showed stability in solving many problems such as the static and Quasi-static problems (Simulia 2013). For the static model using dynamic analysis, it is recommended that the inertial effects could be reduced by making the mass density bigger or by using the slow rate of loading to limit the oscillation (Mercan 2011).

3.1 Models to simulate cracking in concrete (NC and UHPFRC)

Many models are available in the literature to simulate the behaviour of concrete. These include the discrete crack and smeared crack models, the inner softening band and the concrete damage plasticity model (CDP). The CDP is the most commonly used model for capturing the behaviour of concrete by many researchers such as (Roth *et al.* 2010, Thirumalaiselvi *et al.* 2016, Rama *et al.* 2017, Al-Osta *et al.* 2018, Bahraq *et al.* 2019, Sakr *et al.* 2019). It was developed by Lubliner *et al.* (1989) and Lee and Fenves (1998). In this study, the CDP is a constitutive model

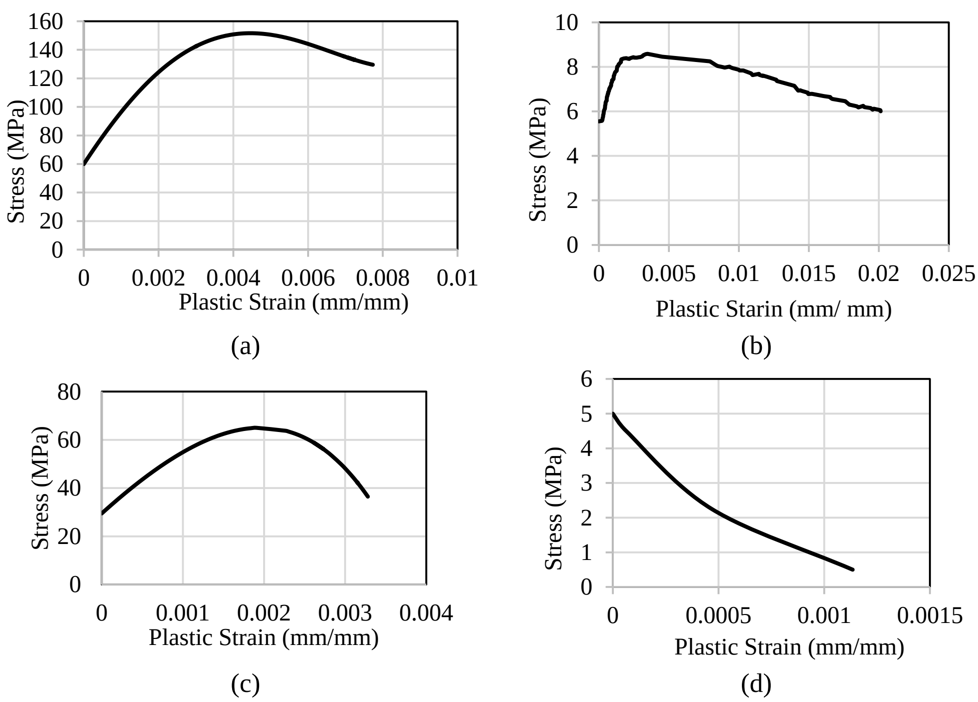

Fig. 9 Nonlinear stress-strain curves: (a) UHPFRC in compression (b) UHPFRC in tension (c) NC in compression (d) NC in tension

available in the ABAQUS software that was also adopted to numerically simulate the behaviour of both NC and UHPFRC concrete. In the CDP, the materials were defined by inputting the parameters shown in Table 6. The uniaxial nonlinear stress-strain of both the NC and UHPRFC concrete under compressive and tensile loading and damage parameters d_c and d_t for the compressive and tension load, respectively, were used to identify the damage pattern and compare them with an experimental one. The uniaxial nonlinear stress-strain relations in compression and tension of the UHPFRC were obtained experimentally by testing cylinder specimens and dogbone specimens, respectively (Figs. 9(a) and 9(b)). Similarly, the nonlinear stress-strain curve for the NC in compression was obtained by testing cylinder specimens, as shown in Figs. 9(c) and 9(d). For the tension behaviour of NC that was used in the FEM, first, the splitting tensile strength test was used to measure the modulus of the rupture, f_t of NC. Thereafter, the full tensile stress-strain of the NC was obtained by assuming that the NC in tension is linear elastic up to cracking at f_t, followed by the linear softening part as given by Bossio *et al.* (2015), and shown in Fig. 9(d). d_c and d_t were obtained by using Eqs. (1) and (2) as given by Birtel and Mark (2006):

The concrete damage parameters in compression and tension to be used in the model are given as

$$d_c = 1 - \frac{\sigma_c {E_c}^{-1}}{\varepsilon_c^{\mathrm{pl}}(1/b_c - 1) + \sigma_c {E_c}^{-1}} \tag{1}$$

$$d_t = 1 - \frac{\sigma_t {E_c}^{-1}}{\varepsilon_t^{\mathrm{pl}}(1/b_t - 1) + \sigma_t {E_c}^{-1}} \tag{2}$$

where: d_c and d_t are the concrete damage in compression and in tension, respectively; σ_c and σ_t are the compressive and tensile stresses, respectively; E_c= concrete elastic modulus; ε_c^{pl} and ε_t^{pl} are the plastic strain coinciding with the compressive and tensile stresses.

where: σ_{b0}/σ_{c0} is the ratio of the initial biaxial compressive stress to the initial uniaxial compressive stress; K is the ratio of the second stress invariant on the tensile meridian (TM) to that on the compressive meridian (CM). σ_{b0}/σ_{c0}, the eccentricity and K values in Table 6 are used as suggested by (Simulia 2013).

3.2 Modelling of the reinforcing rebars and the bond with concrete

The behaviour of steel rebars and stirrups is assumed an elastic-perfectly plastic relationship with parameters that were measured experimentally as mentioned in Section 2.2.1. Both steel rebars and stirrups are embedded in the NC as host elements in the ABAQUS. Since the results of bond in Section 2.2.5 showed that the UHPFRC has admirable bonding with the surface of the NC and the experimental test of the retrofitted beams showed that no debonding was observed between the NC and the UHPFRC, the bond in FEM was considered to be a perfect bond (surface-based tie constraint). This constraint is used to make all degrees of freedom are equal so that no relative motion between them are found. It can be defined by selecting one surface to act as slave and the other surface to be considered as master surface. The master-slave contact algorithm in ABAQUS is considered to ensure that the nodes on the slave surface (UHPFRC) cannot penetrate the master surfaces (NC).

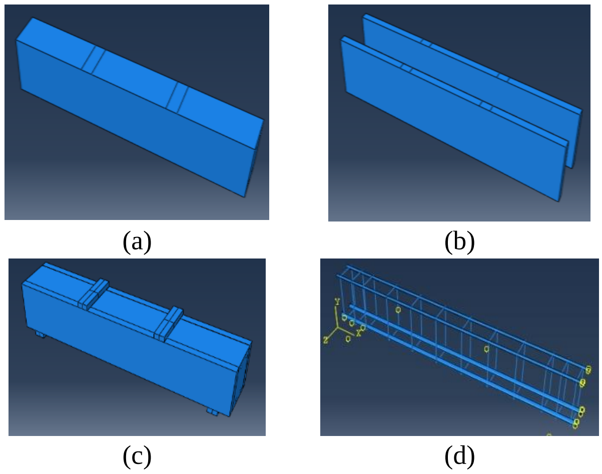

Fig. 10 Geometry of the retrofitted beams: (a) NC beam, (b) UHPFRC strips of RC-2SJ, (c) retrofitted beam, (d) Steel rebars

3.3 Geometry model

The geometry of the beams with different parts, such as the NC beam, the UHPFRC strips of RC-2SJ, the retrofitted beam and the steel rebars, is shown in Fig. 10. In this study, NC, UHPFRC concrete, the bottom and top main longitudinal steel rebars have been modelled using a 3D- 8-noded linear brick element. However, two nodes linear 3D truss element was used to model stirrups.

4. Results and discussion

4.1 Experimental results

4.1.1 Strength of control specimens

The capacity loads for all the control specimens obtained from the experimental work, P_{ex}, are shown in Table 7. The experimental failure loads were compared with the theoretical capacity loads of the control specimens in the shear and flexural, P_{thsN}, P_{thfN}, respectively. The values of P_{thsN} and P_{thfN} were calculated from conventional mechanics (McCormac and Brown 2015) with material properties as mentioned in Section 2.2 under certain assumptions. The non-simplified Eq. (3), provided by ACI 318-14, was used to calculate the shear capacity (V_c) of the control RC beam specimens.

$$V_c = \left(0.16\sqrt{f_c'} + 17\rho_w \frac{V_u\, d}{M_u}\right) b_w\, d \tag{3}$$

$$V_s = \frac{A_v\, f_y\, d}{S} \tag{4}$$

$$P_{thsN} = 2(V_s + V_c) \tag{5}$$

where: f_c' is the compressive strength of NC after 28-day of curing (in MPa), ρ_w is the percentage of longitudinal reinforcement, V_u and M_u are the shear and moment at the intended section, and d and b_w are the effective depth and width, respectively, of the beam's cross-section. A_v is the cross-sectional area of the stirrup, f_y is the yield strength of the stirrup, and S is the spacing between the stirrups.

For the flexural strength, it was assumed that (i) the strain distribution is linear across the depth and the ultimate strain of concrete, ε_{cu}=0.003, (ii) the magnitude of rectangular stress in compression is taken as 0.85 fc' and (iii) the reinforcing steel is perfectly elastic-plastic. From Table 7, it can be observed that there are small differences between the theoretical shear strength and the experimental failure loads of the control RC beam specimens thereby proving that the failure mode of the control specimens is shear, which is as expected.

Table 7 Capacity of control specimens

Specimen	f_{uc} [MPa]	fc' [MPa]	h_{uc} mm	t mm	Load capacity in [kN]: Experimental, P_{ex}	Theoretical: shear, P_{thsN} and P_{thsR}	Theoretical: flexural, P_{thfN} and P_{thfR}	% Error*
RC- CT-1.0	-	65	-	-	383	345	641	-9.9
RC-2SJ-1.0	151.4		230	30	529	530	721	0.3
RC-3SJ-1.0			260		625	556	810	-11.0
RC- CT-1.5	-		-	-	286	275	458	-3.8
RC-2SJ-1.5	151.4		230	30	435	439	515	1.0
RC-3SJ-1.5			260		487	462	578	-5.1

*100×(P_{thsR}-P_{ex})/P_{ex}

4.1.2 Strength of retrofitted specimens

The failure load of the retrofitted specimens obtained from the experimental work, P_{ex}, is presented in Table 7. For the theoretical flexural strength of the retrofitted RC beam from two sides and three sides, P_{thfR} was obtained from the principle applied and given by Al-Osta *et al.* (2017).

The empirical model for theoretical shear capacity, P_{thsR}, of a beam retrofitted by UHPFRC layers can be obtained by adding the shear contribution of UHPFRC layers to the nominal shear strength resulting from the normal concrete and shear reinforcement (i.e., stirrups). The equation for shear strength of a RC beam having shear reinforcement and retrofitted by UHPFRC layers can be expressed as follows by adding the shear contribution of UHPFRC jacketing to the basic ACI Eqs. (3) and (4)

$$V_T = V_c + V_s + V_{UH} \tag{6}$$

where: V_T is the total shear strength of beam including the effect of retrofitting, and V_{UH} representing the UHPFRC contribution towards shear resistance. The expression for V_{UH} can be given as

$$V_{UH} = \sqrt{f_{uc}}\left(\frac{d}{a}\right)^{A}\left(\frac{h_{uc}}{t}\right)^{B} h_{uc}\, t \tag{7}$$

where: f_{uc} is the compressive strength of UHPFRC (in MPa), a/d is the shear span to depth ratio, h_{uc} and t are the overall depth and the thickness of the retrofitting layers. A and B are the empirical constants that need to be determined using the regression of experimental data.

The experimental data obtained through the present study, as presented in Table 7, were used to best-fit Eq. (7) for V_{UH}. The best-fitted values of the empirical constants A and B used in Eq. (7), determined through the regression analysis of the experimental data results, are as follows: A=0.36 and B=0.055. Thus, by substituting these constants, the following empirical model for V_{UH} can be given as

$$V_{UH} = \sqrt{f_{uc}}\left(\frac{d}{a}\right)^{0.36}\left(\frac{h_{uc}}{t}\right)^{0.055} h_{uc}\, t \tag{8}$$

$$P_{thsR} = 2(V_s + V_c + V_{UH}) \tag{9}$$

The theoretical shear capacity, P_{thsR}, of the retrofitted beams calculated using Eq. (9) is presented in Table 7 along with the experimental values of the shear capacities of these beams. It is clear that there are small differences between the theoretical shear strength and the experimental failure loads of all beams.

4.1.2.1 Data of Runao et al. and Sakr et al.

The proposed model for estimating the failure load of the retrofitted beams was validated with the available experimental results that were reported by Ruano *et al*. (2015), Sakr *et al*. (2019). The RC beams (B7, B8, B13 and B14) tested by Runao *et al*. were repaired using layers of 30 mm thickness over three surfaces of beams made of steel fiber reinforced concrete (SFRC). The beams have a length of 1600 mm, and a cross-section of 250 mm height and 150 mm width, in addition to being reinforced in the bottom and top with 3ø16mm and 2ø8 mm, respectively. Stirrups with a diameter of 6mm at a spacing of 125 mm center to center were used as a shear reinforcement. The beams (ST-2S and ST-2S-R) tested by Sakr, Sleemah *et al*. were retrofitted using layers of 30 mm thickness over two surfaces of beams made of UHPFRC. The beams have a length of 2000 mm, and a cross-section of 300 mm height and 150 mm width, in addition to being reinforced in the bottom and top with 2ø18mm and 2ø10 mm, respectively. Stirrups with a diameter of 8mm at a spacing of 400 mm center to center were used as a shear reinforcement. The predicted values of P_{thsR} for the six repaired RC beams were estimated by using Eqs (8) and (9). The details of the comparison between the experimental and predicted values of the repaired specimens are listed in Table 8. It can be seen that, with the exception of one specimen, the predicted failure loads differ by less than 10% from the experimental results, lending confidence to the prediction of the contribution of UHPFRC layers towards shear capacity of the retrofitted beams.

4.1.3 RC Beams with a/d=1.0

All beam specimens in this category were tested with a shear span of a=200 mm so that the ratio of a/d=1.0. The control specimen RC- CT-1.0 showed the typical flexural hair vertical cracks at the midspan of the beam at a load of 145 kN, as can be seen in Fig. 11(a). Thereafter, as the load increased, diagonal shear cracks started to develop and spread over the shear span of 200 mm towards the supports at a load of 248 kN. Finally, the beams failed in shear mode as can be observed from Fig. 11(a). Fig. 12 also shows the

Table 8 Comparison of predicted values with Runao *et al.* (2015), Sakr *et al.* (2019) data

Researcher	Specimen	f_{uc} [MPa]	f_c' [MPa]	a/d	h_{uc} [mm]	t	Load capacity in [kN] Experimental P_{ex}	Load capacity in [kN] Predicted shear strength P_{thsR}	% Error *
Ruano *et al.* (2015)	B7	86.5	26.3	1.73	280	30	278.5	291.7	4.7
	B8						276.2	291.7	5.6
	B13	95.5					262.4	299	14
	B14						298	299	0.3
Sakr *et al.* (2019)	ST-2S	137.4	30	1.97	300		281	301	7.2
	ST-2S-R						331	301	-9.0

*100 × (P_{thsR}-P_{ex})/P_{ex}

load-deflection curve and indicates a sudden failure after achieving the maximum load of 383 kN with a corresponding displacement of 2.17 mm. The strain of normal concrete in the top of the middle part was found to be in the neighborhood of 0.0011 (Fig. 13), and this confirmed the failure of the beam in shear. For the beam (RC-2SJ-1.0) that was retrofitted on both sides using the epoxy adhesive, the first crack was initiated in the RC-2SJ-1.0 specimen at a load that was double the load for the first crack in the control specimen. Cracks were concentrated in the middle 960 mm span of the beam, as shown in Fig. 12. This may be attributed to the extra flexural strength of the retrofitted RC beam provided by the UHPFRC jackets. Thereafter, the flexure-shear cracks were initiated and become wider as the load increased until the failure occurred at the ultimate load of 529 kN (38% more than the control beam). At the level of this ultimate load, the strain of compression on the NC at the middle part was 0.00172 (Fig. 13) which indicated that the beam was close to failure in flexure. In general, RC-2SJ-1.0 showed a fewer number of cracks, as compared to the control beams (Fig. 11(b)). In addition, the retrofitted beam had gained a slight ductile behaviour with remarked stiffness as compared to the control one, as shown in Fig. 12. At the failure stage, it was observed that the retrofitted strips were completely attached to the substrate beam without any debonding. Therefore, the core beam failed in shear prior to developing the full capacity of the UHPFRC jacketing, as was also confirmed by the load deflection curve of the composite beam in Fig. 12.

For the RC beam (RC-3SJ-1.0) that was retrofitted in three sides (U-Jacketing) using epoxy adhesive, the epoxy-bonded beam (RC-3SJ-1.0) failed in flexural-shear mode at a max load of 625kN. Although, the RC-3SJ-1.0 has a confining jackets in both the bottom and the longitudinal sides, it behaves in a similar way to that of the two-sided jacketing. The RC-3SJ-1.0 exhibits superior performance for failure load, stiffness, ductility and the number of cracks, as compared to previous specimens (Figs. 11(c) and 12). Even though the beams failed under a relatively high load, no debonding had occurred between the substrate and the UHPFRC. However, one problem was observed with the retrofitted beam in the three-sided jacketing using an epoxy adhesive, which was a mismatch between the

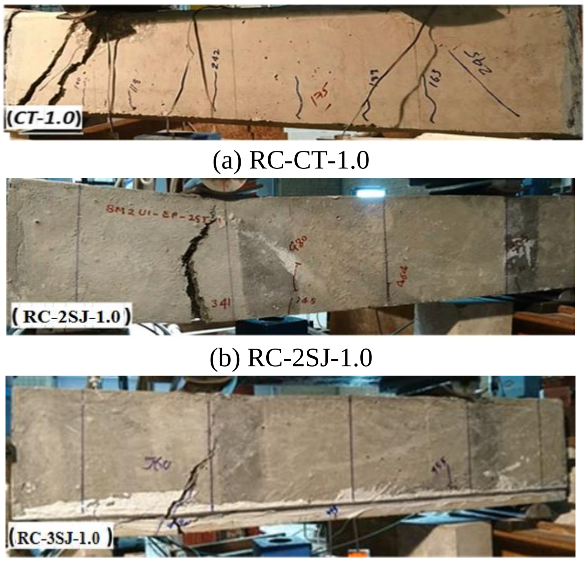

(a) RC-CT-1.0

(b) RC-2SJ-1.0

(c) RC-3SJ-1.0

Fig. 11 Crack patterns at failure stage of RC beam specimens with *a/d*=1.0

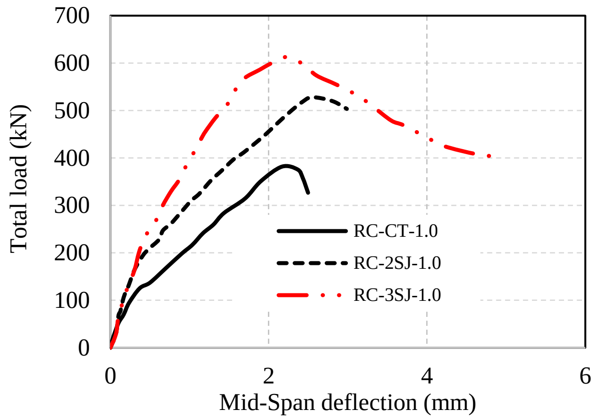

Fig. 12 Load-deflection curves of RC beam specimens with *a/d*=1.0

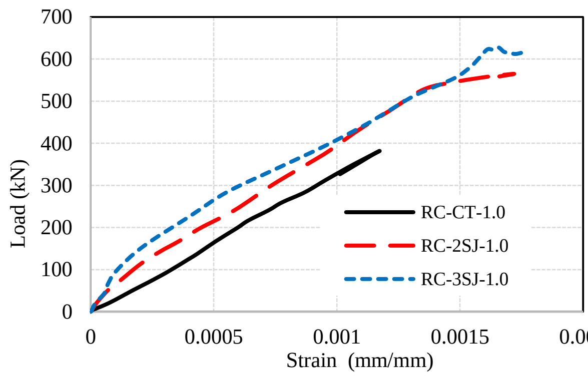

Fig. 13 Load vs. compressive strain of concrete in beam specimens with *a/d*=1.0

bottom-retrofitted layers and the other two layers, Fig. 11(c). This created a disjointedness in the jacketing and, as a result, the deformation capacity after reaching peak load was not effective thereby leading to the failure of the composite beam in the flexure-shear failure, as shown in

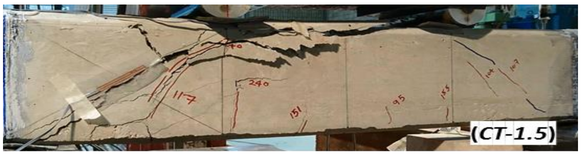

(a) RC-CT-1.5

(b) RC-2SJ-1.5

(c) RC-3SJ-1.5

Fig. 14 Crack patterns at failure stage of RC beam specimens with *a/d*=1.5

Fig. 12. It can be seen that there is definite evidence of softening that was not present for the RC-2SJ-1.0 or the control specimens.

4.1.4 Test Beams with a/d=1.5

In this category, the beams were tested with a shear-span of (*a*=280 mm) to maintain a ratio of *a/d*=1.5. The RC-CT-1.5 showed flexural cracks at the midspan which were initiated at a load of 45 kN, as shown in Fig. 14(a). The first oblique crack was initiated at a load of 107 kN, and with a further increase in the load, the beam failed suddenly in shear, the cracks being propagated at the farthest locations from the supports until the failure of the beam. The ultimate load was 286 kN, which is less than that in (RC-CT-1.5) by 33%. This occurred because the shear span in this case (*a/d*=1.5) was shifted from the support, therefore, the wide-spacing stirrups were included within the shear span. Moreover, at a higher *a/d* ratio, the effectiveness of the arch action and dowel action is less, which results in a lower shear strength. The load-deflection response (Fig. 15) of the beam clearly shows a softening part after reaching peak load that represents the shear failure. The value of the strain of NC on the compression side in the middle part was in the neighborhood of 0.0014, and that confirmed the failure of the beam in shear.

The beam (RC-2SJ-1.5) showed flexural cracks at a load of 130 kN followed by flexure-shear cracks on the UHPFRC layer, as shown in Fig. 14(b). By further increasing the load, the flexure-shear cracks became wider and the beam failed suddenly at 435 kN. Furthermore, the load-deflection curve shown in Fig. 15 demonstrated that the beam failed in shear. This inconsistency in the behaviour between the beam itself and the load-deflection curve is attributed to the failure of the original beam prior to the retrofitted layers of the UHPFRC. Therefore, the load-deflection curve gives an effective representation of the composite action of the behaviour of this type of retrofitted beam. The collapse load of the beam (RC-2SJ-1.5) was 435 kN, with an average increase in shear strength of 46% as compared to the beam specimen (RC-CT-1.5).

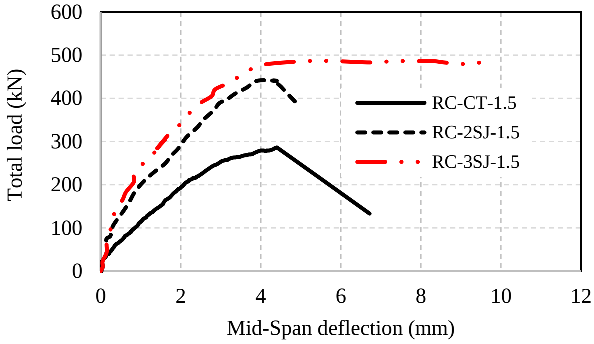

Fig. 15 Load-deflection curves of RC beam specimens with *a/d*=1.5

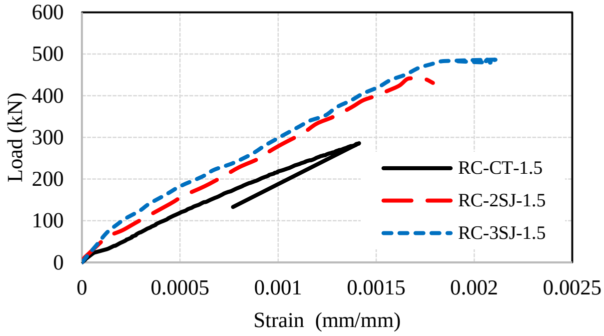

Fig. 16 Load vs. compressive strain of concrete in beam specimens with *a/d*=1.5

The beam (RC-3SJ-1.5) showed flexural cracks that were initiated at a load of 250 kN and propagated as can be seen Fig. 14(c). Thereafter, by increasing the load, the beam failed in pure flexure at a peak load of 487 kN with an average increase of 69%. In addition, the load-deflection curves of the beam showed an improvement in stiffness as shown in Fig. 15. This beam shows excessive ductility and then reaches a plateau. At the ultimate load of beam (RC-3SJ-1.5), the strain in compression of NC at the middle part was 0.0021 (Fig. 16), which indicated that the beam was near to failure in flexure. In this case, the failure of the control beam has managed to convert the brittle shear response of the original beam into a ductile, flexure type failure, which is the best scenario that the repair engineer can hope for.

4.1.5 Summary of the results

Table 9 shows the summary of the experimental failure loads as well as the failure modes of the tested specimens. It can be seen that there is an increase in the failure load of the retrofitted beams of about 38% to 70%. This confirms that the UHPFRC strips can be used effectively as external layers to enhance the performance in the failure load, stiffness and number of cracks of the deficient RC beams. Further, there was an improvement in performance of the behaviour of the beams that were retrofitted in three sides. It was also found that all of the retrofitted beams showed fewer cracks as compared to the control beams. This can be ascribed to the higher tensile strength of both the UHPFRC

Table 9 Summary of Results of Experimental Work

Specimen Designation	*a/d* ratio	Exp. Failure Load [kN]	Failure Load Increasing [%]	Failure Mode
RC-CT-1.0		383	0	Shear
RC-2SJ-1.0	1.0	529	38	Shear
RC-3SJ-1.0		625	63	Flexure-Shear
RC-CT-1.5		286	0	Shear
RC-2SJ-1.5	1.5	435	52	Shear
RC-3SJ-1.5		487	70	Flexural

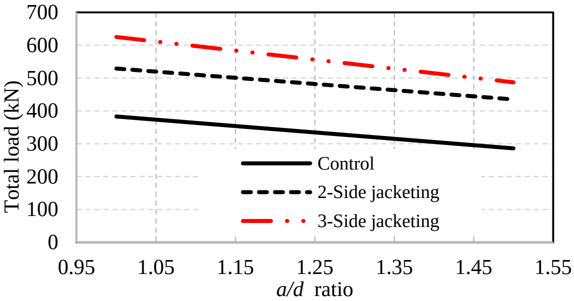

Fig. 17 Effect of the *a/d* ratio and retrofitting the jacketing on the failure load

layers and the epoxy adhesive which prevented the hair cracks from developing through the epoxy adhesive or the UHPFRC layers. The effect of the *a/d* ratio and the retrofitting configurations on the failure load of the RC beams is presented in Fig. 17.

4.2 FEM results

The FEM developed was validated using the experimental tests for the RC beams as described above that consist of both the control and the retrofitted RC beams samples. The load vs. deflection curves and damage patterns from the experimental FEM works were compared.

4.2.1 Control specimens

For the control beams, the RC beams (RC-CT-1.0 and RC-CT-1.5), the predicted load vs. deflection curves at mid-span by FEM, and the experimental work are shown in Figs. 18a and 18b. It can be seen that the total response of both control beams RC-CT-1.0 and RC-CT-1.5 is in good coincidence with the experiment. The FEM predicted failure load capacities of the beams are 377 kN and 295 kN, which are 2% lower and 3.1% higher than the experimental test values of 383 kN and 286 kN. The values of the ultimate load capacities of the RC beams obtained from the FEM and the experimental work were also compared with the values obtained from ACI-318-14, as can be seen in Table 7. It is to be noted that the ultimate values of the loads are in close agreement with the ACI-318-14 equation. Furthermore, the failure mode from the FEM for both beams RC-CT-1.0 and RC-CT-1.5 is a diagonal tension crack as observed from the results of the experimental work (Fig. 19).

4.2.2 Retrofitted specimens

Similarly, the FE prediction of the failure loads for RC

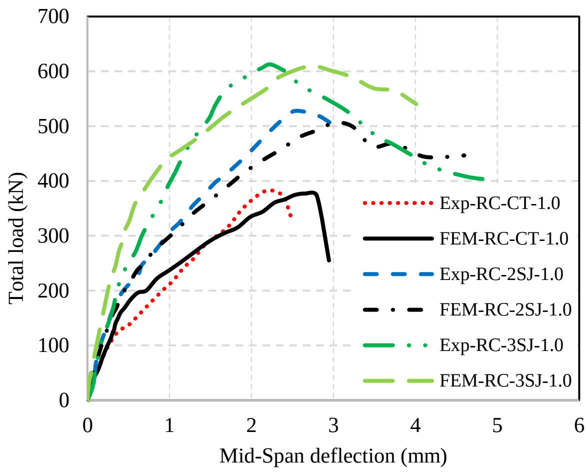

(a) *a/d* = 1.0

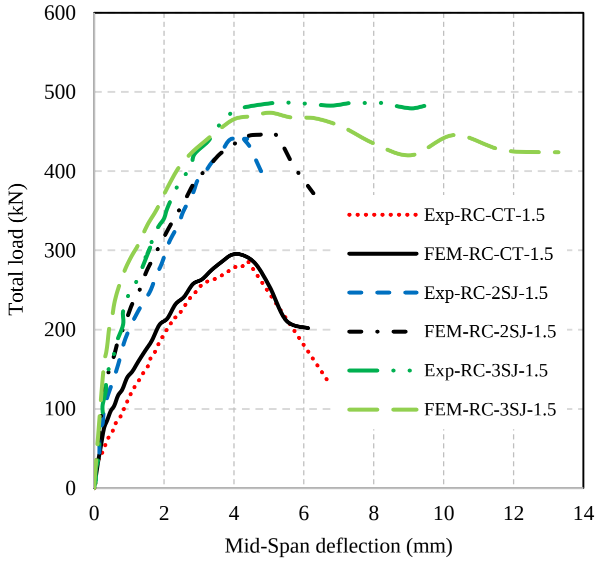

(b) *a/d* = 1.5

Fig. 18 Experimental and FEM load deflection curves of beams with (a) *a/d*=1.0 and (b) *a/d* =1.5

retrofitted beams (RC-2SJ-1.0, RC-3SJ-1.0, RC-2SJ-1.5 and RC-3SJ-1.5) is 506 kN, 609 kN, 446 kN and 474 kN. This was found to be in good coincidence with the experimental failure values of 529 kN, 625 kN, 435 kN and 487 kN, respectively. It can be seen that the FE analysis is 4.4% and 2.6% lower in the case of the RC-2SJ-1.0 and RC-3SJ-1.0 specimens, respectively, and is 2.6% higher and 2.7% lower for the RC-2SJ-1.5 and RC-3SJ-1.5 specimens, respectively, when compared with the corresponding experimental values. The overall response of the retrofitted specimens obtained from FE analysis and the experimental work were found to be in close agreement with each other, as can been seen from Fig. 18(b). The load vs. deflection curves obtained from the FE is slightly different from the curves obtained from the experimental work. This can be ascribed to the bond between the NC and UHPFRC layers in the FEM that was assumed to be perfect. However, bubbles that may have been produced in the epoxy resulted in the gaps between the UHPFRC plates and the NC substrate surface.

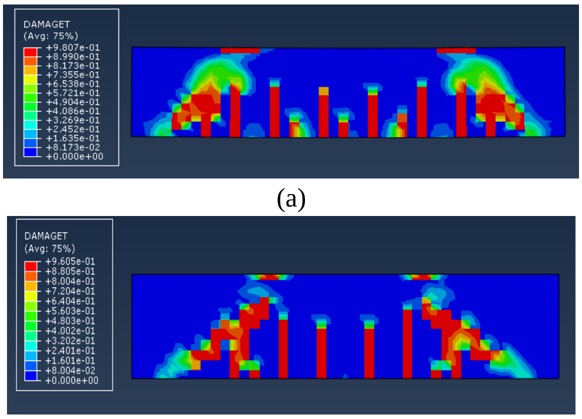

(a)

(b)

Fig. 19 Crack pattern of control beams at failure stage: (a) RC-CT-1.0 (b) RC-CT-1.5

5. Conclusions

Based on the results of the experimental investigation and numerical modelling presented in this paper, the following conclusions could be obtained:

• Bonding of the UHPFRC strips using epoxy adhesives could be easily used in practice to enhance or strengthen the RC beams without causing debonding of the UHPFRC strips from the substrate, even at relatively high loads.

• Based on the observed reduction in the mid-span deflections of the retrofitted RC beams, using UHPFRC strips to strengthen the RC beams could increase the stiffness of the beams under service conditions.

• The retrofitting of the RC beams using UHPFRC strips could increase the initial cracking load and ductility, in addition to reducing the number of cracks.

• Beams retrofitted with UHPFRC strips on two faces exhibited the lowest level of capacity improvement, whereas the beams retrofitted on three faces showed a higher enhancement.

• Retrofitting the RC beams on the two side faces could shift the failure mode from shear to flexure-shear with an enhancement in the failure load of 38% to 52 % and a slight increase in stiffness.

• Retrofitting the RC beams on three faces could shift the failure pattern from shear failure to flexure-shear and pure flexure failures with *a/d*=1.0 and 1.50, respectively, in addition to increasing the failure load by up to 70%.

• RC beams retrofitted on three faces with UHPFRC strips at *a/d*=1.5 exhibited ductile failure behaviour.

• The level of enhancement in the load carrying capacity of the retrofitted RC beams increases with increasing *a/d* ratios.

• Retrofitting of the RC beams on the sides alone greatly enhances the shear strength of the beams, although there is no notable change in the ductility of the member. However, adding the UHPFRC strip on the bottom face of the beam has a profound influence on the ductility of the member in both shear span cases. For beam with *a/d*=1.5, there is a complete transformation in the failure pattern from brittle shear to the highly desirable ductile flexural mode of failure.

• The bottom layer of UHPFRC, when highly stressed in tension, increases tensile strain levels to magnitudes that cause the strain in the main reinforcement to exceed its yield strain. It is this inherent ability of the UHPFRC to tolerate very high tensile strains that makes it a desirable and complementary material to be used in unison with the main reinforcement of the RC beam sections.

• A proposed model to predict the failure capacity of the retrofitted RC beams evolved by using a multi-level regression of the test data was presented. The accuracy of the predicted values of the strength has been validated by comparing the results of the developed model with the available experimental data.

• The results obtained from the FEM for the overall response of the retrofitted RC beams were in good agreement with the experimental test results. It is clear that the FEM using CDP model could be used to estimate both the peak load and the load-deflection response of both the control and retrofitted RC beams.

Acknowledgments

The author would like to acknowledge the support provided by the Deanship of Scientific Research (DSR) at King Fahd University of Petroleum & Minerals (KFUPM), Saudi Arabia for funding this work through **Project No. IN161055**. The support provided by the Department of Civil and Environmental Engineering is also acknowledged.

References

ACI committee 318 (2014), Building Code Requirements for Structural Concrete and Commentary, ACI 318-14.

ACI-Committee 546 (2014), 546.3R-14: Guide to Materials Selection for Concrete Repair, Farmington Hills, American Concrete Institute.

Ahlborn, T., Harris, D., Misson, D. and Peuse, E. (2011), "Strength and durability characterization of ultra-high performance concrete under variable curing conditions", *Tran. Res. Board Ann. Meet.*, **22**(51), 68-75.

Ahmad, S., Hakeem, I. and Maslehuddin, M. (2016), "Development of an optimum mixture of ultra-high performance concrete", *Eur. J. Environ. Civil Eng.*, **20**(9), 1106-1126. https://doi.org/10.1080/19648189.2015.1090925.

Al-Osta, M., Isa, M., Baluch, M. and Rahman, M. (2017), "Flexural behavior of reinforced concrete beams strengthened with ultra-high performance fiber reinforced concrete", *Constr. Build. Mater.*, **134**, 279-296. https://doi.org/10.1016/j.conbuildmat.2016.12.094.

Al-Osta, M.A., Al-Sakkaf, H.A., Sharif, A.M., Ahmad, S. and Baluch, M.H. (2018), "Finite element modeling of corroded RC beams using cohesive surface bonding approach", *Comput. Concrete*, **22**(2), 167-182. https://doi.org/10.12989/cac.2018.22.2.167.

Al-Osta, M.A. (2018) , "Exploitation of ultra-high performance fibre reinforced concrete for the strengthening of concrete structural members", *Adv. Civil Eng.*, **2018**, Article ID 8678124, 1-12. https://doi.org/10.1155/2018/8678124.

ASTM International (2017), ASTM C39 Standard Test Method for

Compressive Strength of Cylindrical Concrete Specimens, ASTM International, West Conshohocken, PA.

ASTM International (2016), ASTM C78/C78M-15b Standard Test Method for Flexural Strength of Concrete (Using Simple Beam with Third-Point Loading), ASTM International, West Conshohocken, PA.

ASTM International (2004), ASTM C496/C496M Standard Test Method for Splitting Tensile Strength of Cylindrical Concrete, ASTM International, West Conshohocken, PA.

ASTM International. (2013). ASTM C882-99 Standard Test Method for Bond Strength of Epoxy-Resin Systems used with Concrete, ASTM International, West Conshohocken, PA:.

Bahraq, A.A., Al-Osta, M.A., Ahmad, S., Al-Zahrani, M.M., Al-Dulaijan, S.O. and Rahman, M.K. (2019), "Experimental and numerical investigation of shear behavior of RC beams strengthened by ultra-high performance concrete", *Int. J. Concrete Struct. Mater.*, **13**(1), 1-19. https://doi.org/10.1186/s40069-018-0330-z.

Birtel, V. and Mark, P. (2006), "Parameterised finite element modelling of RC beam shear failure", *ABAQUS Users' Conference*.

Bossio, A., Monetta, T., Bellucci, F., Lignola, G.P. and Prota, A. (2015), "Modeling of concrete cracking due to corrosion process of reinforcement bars", *Cement Concrete Res.*, **71**, 78-92. https://doi.org/10.1016/j.cemconres.2015.01.010.

Chalioris, C.E., Thermou, G.E. and Pantazopoulou, S.J. (2014), "Behaviour of rehabilitated RC beams with self-compacting concrete jacketing-Analytical model and test results", *Constr. Build. Mater.*, **55**, 257-273. https://doi.org/10.1016/j.conbuildmat.2014.01.031.

Chen, J. and Tao, Y. (2011), "Finite element modelling of FRP-to-concrete bond behaviour using the concrete damage plasticity theory combined with a plastic degradation model", *Advances in FRP Composites in Civil Engineering*, Springer, Berlin, Heidelberg. https://doi.org/10.1007/978-3-642-17487-2_7.

Chynoweth, G., Stankie, R.R., Allen, W.L., Anderson, R.R., Babcock, W.N., Barlow, P., Bartholomew, J.J., Bergemann, G.O., Bullock R.E. and Constantino, F.J. (1996), "Concrete repair guide", *ACI Committee, Concrete Repair Manual*, **546**, 287-327.

Graybeal, B. (2011), "FHWA TECHNOTE, ultra high performance concrete", FHWA Publication No, FHWA-HRT-11-038, Federal Highway Administration.

Graybeal, B.A. (2006), "Material property characterization of ultra-high performance concrete", No. FHWA-HRT-06-103. United States, Federal Highway Administration, Office of Infrastructure Research and Development.

Hakeem, I.Y.A. (2011), "Characterization of an ultra-high performance concrete", MS Thesis, King Fahd University of Petroleum and Minerals, Saudi Arabia.

Hussein, L. and Amleh, L. (2015), "Structural behavior of ultra-high performance fiber reinforced concrete-normal strength concrete or high strength concrete composite members", C*onstr. Build. Mater.*, **93**, 1105-1116. https://doi.org/10.1016/j.conbuildmat.2015.05.030.

Khan, U., Al-Osta, M.A. and Ibrahim, A. (2017), "Modeling shear behavior of reinforced concrete beams strengthened with externally bonded CFRP sheets", *Struct. Eng. Mech.*, **61**(1), 125-142. https://doi.org/10.12989/sem.2017.61.1.125.

Lee, J. and Fenves, G.L. (1998), "Plastic-damage model for cyclic loading of concrete structures", *J. Eng. Mech.*, **124**(8), 892-900. https://doi.org/10.1061/(ASCE)0733-9399(1998)124:8(892).

Lubbers, A.R. (2003), "Bond performance between ultra-high performance concrete and prestressing strands", PhD Dissertation, Ohio University.

Lubliner, J., Oliver, J., Oller, S. and Onate, E. (1989), "A plastic-damage model for concrete", *Int. J. Solid. Struct.*, **25**(3), 299-326. https://doi.org/10.1016/0020-7683(89)90050-4.

McCormac, J.C. and Brown, R.H. (2015), *Design of Reinforced Concrete*, John Wiley & Sons.

Mercan, B. (2011), "Modeling and behavior of prestressed concrete spandrel beams", PhD Dissertation, University of Minnesota.

Mohammed, T.J., Bakar, B.A. and Bunnori, N.M. (2016), "Torsional improvement of reinforced concrete beams using ultra high-performance fiber reinforced concrete (UHPFC) jackets-Experimental study", *Constr. Build. Mater.*, **106**, 533-542. https://doi.org/10.1016/j.conbuildmat.2015.12.160.

Noshiravani, T. and Brühwiler, E. (2013), "Experimental investigation on reinforced ultra-high-performance fiber-reinforced concrete composite beams subjected to combined bending and shear", *ACI Struct. J.*, **110**(2), 251.

Ombres, L. (2015), "Structural performances of reinforced concrete beams strengthened in shear with a cement based fiber composite material", *Compos. Struct.*, **122**, 316-329. https://doi.org/10.1016/j.compstruct.2014.11.059.

Rahman, S., Molyneaux, T. and Patnaikuni, I. (2005), "Ultra high performance concrete, recent applications and research", *Aust. J. Civil Eng.*, **2**(1), 13-20. https://doi.org/10.1080/14488353.2005.11463913.

Rama, J.S., Chauhan, D.R., Sivakumar, M.V.N., Vasan, A. and Murthy, A.R. (2017), "Fracture properties of concrete using damaged plasticity model-A parametric study", *Struct. Eng. Mech.*, **64**(1), 59-69. https://doi.org/10.12989/sem.2017.64.1.059.

Roth, M.J., Slawson, T.R. and Flores, O.G. (2010), "Flexural and tensile properties of a glass fiber-reinforced ultra-high-strength concrete, an experimental, micromechanical and numerical study", *Comput. Concrete*, **7**(2), 169-190. https://doi.org/10.12989/cac.2010.7.2.169.

Ruano, G., Isla F., Pedraza, R.I., Sfer, D. and Luccioni, B. (2014), "Shear retrofitting of reinforced concrete beams with steel fiber reinforced concrete", *Constr. Build. Mater.*, **54**, 646-658. https://doi.org/10.1016/j.conbuildmat.2013.12.092.

Ruano, G., Isla, F., Sfer, D. and Luccioni, B. (2015), "Numerical modeling of reinforced concrete beams repaired and strengthened with SFRC", *Eng. Struct.*, **86**, 168-181. https://doi.org/10.1016/j.engstruct.2014.12.030.

Sakr, M.A., Sleemah, A.A., Khalifa, T.M. and Mansour, W.N. (2019), "Shear strengthening of reinforced concrete beams using prefabricated ultra-high performance fiber reinforced concrete plates, Experimental and numerical investigation", *Struct. Concrete*, 1-17. https://doi.org/10.1002/suco.201800137.

Sika Construction Chemicals (2014), "Sikadur ® -32 LP", Product data sheet.

Simulia, D. (2013), *ABAQUS 6.13 User's Manual*, Dassault Systems, Providence, RI.

Sprinkel, M.M. and Ozyildirim, C. (2000), "Evaluation of high performance concrete overlays placed on Route 60 over Lynnhaven Inlet in Virginia", No. VTRC-01-R1, Virginia Transportation Research Council.

Tai, Y.S., Pan, H.H. and Kung, Y.N. (2011), "Mechanical properties of steel fiber reinforced reactive powder concrete following exposure to high temperature reaching 800 C", *Nucl. Eng. Des.*, **241**(7), 2416-2424. https://doi.org/10.1016/j.nucengdes.2011.04.008.

Thirumalaiselvi, A., Anandavalli, N., Rajasankar, J. and Iyer, N.R. (2016), "Numerical evaluation of deformation capacity of laced steel-concrete composite beams under monotonic loading", *Steel Compos. Struct.*, **20**(1), 167-184. http://dx.doi.org/10.12989/scs.2016.20.1.167.

CC